RSC Advances

PAPER

View Article Online
View Journal | View Issue

Cite this: *RSC Adv.*, 2025, **15**, 37447

Synthesis, biological evaluation, and docking analysis of novel benzimidazole–triazole hybrids as potential anticancer agents

Amir Shervin Shokouhi Asl,[a†] Sara Ranjbar,[b†] Mohammad Hosein Sayahi,[c] Zahra Dehghani,[b] Amir Mohammad Taherkhani,[d] Manica Negahdaripour,[be] Navid Dastyafteh,[d] Mina Emami,[b] Sajedeh Safapoor,[d] Abbas Ghahramani,[f] Mohammad Reza Mohajeri-Tehrani,[d] Bagher Larijani,[d] Mohammad Mahdavi*[d] and Younes Ghasemi*[be]

A series of novel benzimidazole–triazole acetamide hybrids with different substitutions at the acetamide moiety were designed and synthesized in an effort to discover potential anticancer agents. The compounds were evaluated for their *in vitro* antiproliferative and cytotoxicity activities against two cancer cell lines (A549 and SW480) and a normal cell (MRC-5) using the MTT assay. The results revealed that most derivatives exhibited moderate to high levels of antiproliferative activity. Notably, derivative **9f** emerged as the most potent antiproliferative agent with IC_{50} values of 16.1 ± 1.1 and 19.7 ± 2.7 μM against A549 and SW480, respectively. Compound **9f** showed significant selectivity towards A549 (SI = 7.5) and SW480 (SI = 6.1) cancer cells compared to the normal MRC-5. Furthermore, this compound exhibited much lower cytotoxicity than cisplatin and doxorubicin against the normal cells. The effects of **9f** on cell cycle distribution and apoptosis induction in A549 cells were investigated using flow cytometry. The derivative significantly arrested cells in the S phase and remarkably induced apoptosis at the IC_{50} concentration. Compound **9f** was predicted to have suitable pharmacokinetics and low toxic effects as an anticancer candidate drug. The docking study demonstrated that compound **9f** interacted with topoisomerase II-DNA, exhibiting a binding energy comparable to that of etoposide.

Received 20th April 2025
Accepted 28th July 2025

DOI: 10.1039/d5ra02760h

rsc.li/rsc-advances

1. Introduction

Cancer is a critical health issue concerning both diagnosis and treatment, as it stands as the second leading cause of death globally. The number of newly diagnosed cancer cases is estimated to increase by 77% in 2050, reaching 35 million compared to 20 million in 2020.[1] Both genetic and environmental factors contribute to uncontrolled cell proliferation, causing malignancies complicated by the influence of various intracellular signaling pathways. Consequently, several therapeutic approaches, including radiotherapy, surgery, stem cell therapy, bone marrow transplantation, and chemotherapy have been utilized for cancer treatment over the past few decades.[2] However, chemotherapy remains the frontline treatment, particularly in advanced stages. The increase in cancer mortality, the emergence of drug resistance, and the high toxicity of existing chemotherapeutics underscore the urgent need for new anticancer agents.

Benzimidazole is an important pharmacophore in medicinal chemistry[3] due to its amphoteric property and its capability to act as both a hydrogen bond acceptor and donor. This makes it an ideal structure for forming hydrogen bonds with various targets.[4,5] It naturally occurs in the structures of several essential compounds, including vitamin B12, histamine, purine, and biotin.[3,6] Additionally, various substitutions can be added to create new synthetic derivatives. Benzimidazole derivatives exhibit various therapeutic activities, such as antimalarial,[7,8] antipyretic,[9] antihistaminic,[10] anticonvulsant,[11] antimicrobial,[12] antifungal,[13] antioxidant,[14] anthelmintic,[15] and anticancer[16] properties.[3,6,17] Many approved drugs include a benzimidazole nucleus, including pracinostat (a histone deacetylase inhibitor),[18] bendamustine (an alkylating agent),[19] nocodazole (an

[a]*Department of Medicinal Chemistry, School of Pharmacy, Iran University of Medical Sciences, Tehran, Iran*

[b]*Pharmaceutical Sciences Research Center, Shiraz University of Medical Sciences, Shiraz, Iran. E-mail: ghasemiy@sums.ac.ir*

[c]*Department of Chemistry, Payame Noor University, Tehran, Iran*

[d]*Endocrinology and Metabolism Research Center, Endocrinology and Metabolism Clinical Sciences Institute, Tehran University of Medical Sciences, Tehran, Iran. E-mail: momahdavi@tums.ac.ir*

[e]*Department of Pharmaceutical Biotechnology, School of Pharmacy, Shiraz University of Medical Sciences, Iran*

[f]*Department of Pharmaceutical Biotechnology, Faculty of Pharmacy, Kerman University of Medical Sciences, Kerman, Iran*

† These two authors contributed equally to this work, and both are considered as the first authors.

antimitotic agent),[20] dovitinib (a tyrosine kinase inhibitor),[21] binimetinib and selumetinib (both MEK1/2 inhibitor),[22,23] abemaciclib (a CDK inhibitor),[24] veliparib (a PARP inhibitor),[25] galeterone (a steroidal antiandrogen),[26] and nazartinib (an EGFR inhibitor),[27] all of which have demonstrated anticancer activity (Fig. 1). Benzimidazole derivatives exert their anticancer effects through various mechanisms including inducing apoptosis,[28] causing cell cycle arrest,[29] inhibiting the epidermal growth factor receptor (EGFR) and vascular endothelial growth factor receptor (VEGFR),[30] disrupting microtubule polymerization,[31] and inhibiting DNA topoisomerases.[32] In a study by Huynh *et al.* the anticancer potential of certain 2-(substituted phenyl) benzimidazole derivatives was evaluated. They found that 6-methyl-2-(3,4,5-trimethoxyphenyl)-1*H*-benzo[*d*]imidazole (Fig. 1, compound **I**) had the highest cytotoxicity against A549 cells with an IC_{50} value of 39.4 μM.[33] Very recently, we investigated the anticancer activity of *N*-substituted-2-(3,4,5-trimethoxyphenyl)-1*H*-benzo[*d*]imidazole-6-carboxamides. The derivative containing a 2,4-dimethoxyphenyl group (Fig. 1, compound **II**) was discovered to be the most potent anticancer agent.[34]

Triazole is a nitrogen-containing heterocyclic five-membered ring that exists in two isomeric forms: 1,2,3-triazole and 1,2,4-triazole.[35] Triazoles are known for their stability under both oxidizing and reducing conditions, and their ability to form hydrogen bonds, which enhances their solubility and binding affinity towards biomolecular targets.[36] Triazole derivatives show a wide range biological activities, such as antibacterial,[37] antifungal,[38] anticancer,[39,40] antioxidant,[41] antiviral,[42] anti-inflammatory,[43] analgesic,[44] antiepileptic,[11] antihypertensive,[45] antityrosinase,[46–48] antidiabetic,[49] antianxiety,[50] and antitubercular[51] effects. The triazole ring serves as the core structure of several FDA-approved drugs, such as letrozole, ribavirin, fluconazole, rizatriptan, and estazolam. Modifying the substitutions on the triazole core can significantly influence their binding affinity and selectivity towards various biological targets, making them valuable candidates for drug development. Some studies have demonstrated the potential of triazole-acetamide derivatives (Fig. 1, compounds **III** and **IV**) as effective anticancer agents.[52,53]

In recent years, researchers have employed the molecular hybridization approach to design novel drugs with improved potency. Various benzimidazole–triazole hybrids have been developed, and these compounds are known to exhibit a range of biological activities.[54–58] Despite the development of various chemical entities featuring the benzimidazole–triazole structural motif, many of them demonstrate significant anticancer potency.[59]

In this study, a novel series of benzimidazole–triazole acetamide hybrids (Fig. 1, **9a–o**) was designed as potential anticancer agents. 2-(4-((2-(3,4,5-Trimethoxyphenyl)-1*H*-benzo[*d*]imidazol-1-yl)methyl)-1*H*-1,2,3-triazol-1-yl)-*N*-substituted acetamides were synthesized and screened for their antiproliferative activity against cancer cell lines. Moreover, supplementary biological assessments, including cell cycle analysis and apoptosis investigation, were conducted for the most potent derivative. *In silico* assessment of pharmacokinetic and toxicity properties was carried out for the selected derivative. Finally, molecular docking analysis was conducted to estimate the binding affinity and interactions of compounds with the topoisomerase enzyme.

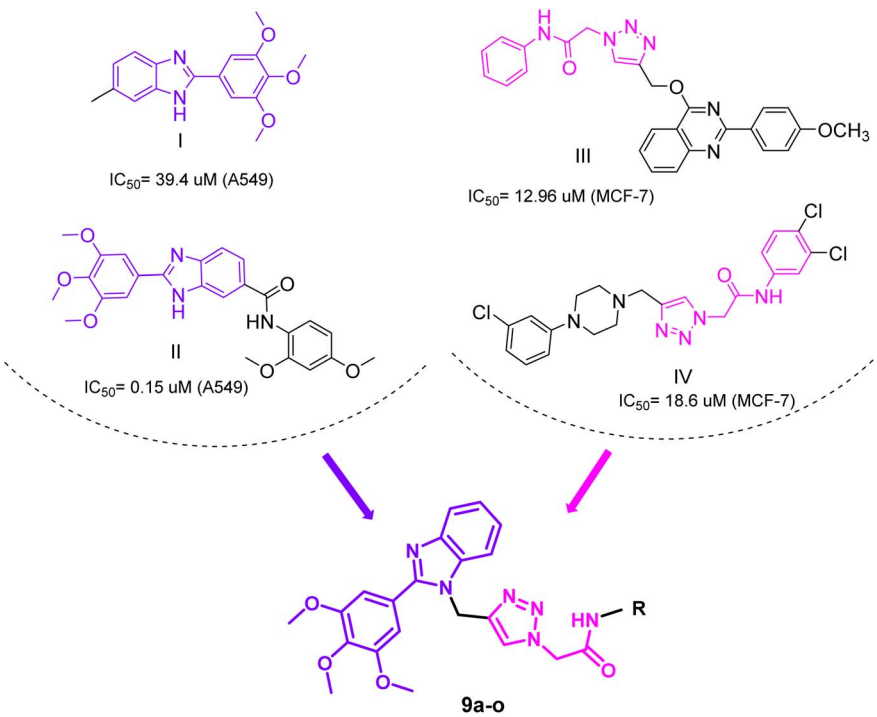

Fig. 1 Rational design of the benzimidazole–triazole hybrids (**9a–o**) as new anticancer agents.

2. Results and discussion

2.1. Synthesis

The synthetic pathway for novel 2-(4-((2-(3,4,5-trimethoxyphenyl)-1*H*-benzo[*d*]imidazol-1-yl)methyl)-1*H*-1,2,3-triazol-1-yl)-*N*-substituted acetamide derivatives (**9a–o**) is illustrated in Scheme 1. The intermediate 2-(3,4,5-trimethoxyphenyl)-1*H*-benzo[*d*]imidazole (**3**) was synthesized by the reaction of 3,4,5-trimethoxybenzaldehyde (**1**) and 1,2-phenylenediamine (**2**) in the presence of sodium metabisulfite in DMF (yield: 92%). Then, the propargylated intermediate (**5**) was prepared by the reaction of compound **3**, potassium carbonate, and propargyl bromide (yield: 90%). The acylation of the corresponding aniline derivative (**6a–o**) with chloroacetyl chloride (**7**) afforded 2-chloro-*N*-substituted acetamide derivatives (**8a–o**) (yield: 80–85%). Finally, the desired compounds (**9a–o**) were synthesized through the three-component click reaction of sodium azide, the corresponding 2-chloro-*N*-substituted acetamide derivatives (**8a–o**), and the propargylated intermediate (**5**) (yield: 74–81%). For the first time, the click reaction of azide–alkyne cycloaddition reaction was carried out by Prof. Sharpless, which enabled him to get the Nobel Prize.[60] The structures of all synthesized compounds were confirmed by ^{1}H NMR, ^{13}C NMR, and IR spectroscopy as well as elemental analysis.

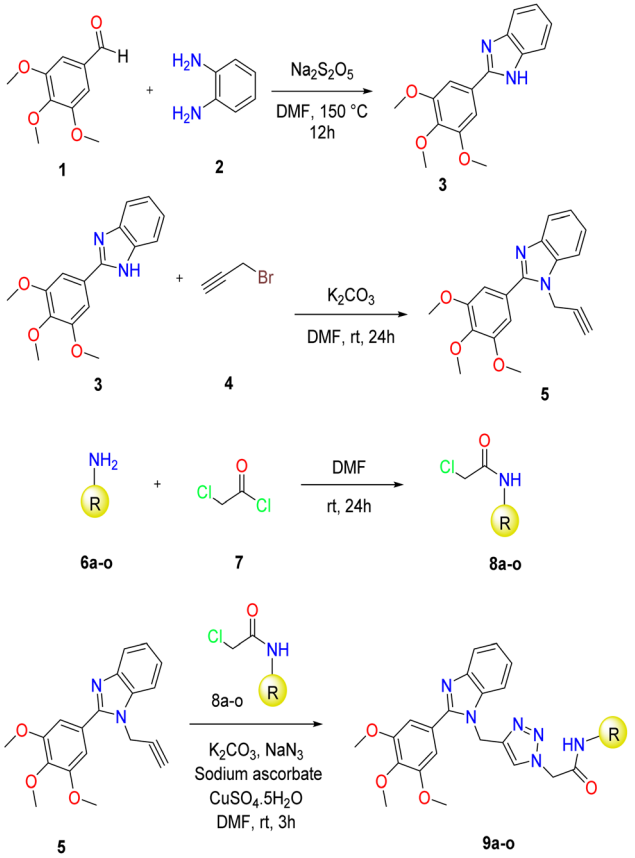

Scheme 1 Procedure for the synthesis of the designed 2-(4-((2-(3,4,5-trimethoxyphenyl)-1*H*-benzo[*d*]imidazol-1-yl)methyl)-1*H*-1,2,3-triazol-1-yl)-*N*-substituted acetamides (**9a–o**).

Table 1 Cytotoxicity of the synthesized compounds against cancer cell lines

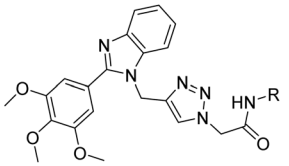

Compound	R	IC_{50}[a] (μM) A549[b]	SW480[c]
9a	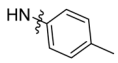	67.4 ± 3.4	77.2 ± 3.2
9b		114.5 ± 5.0	157.5 ± 7.8
9c	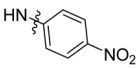	23.5 ± 3.6	22.5 ± 3.9
9d	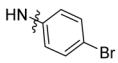	>200	>200
9e		22.2 ± 4.0	30.4 ± 3.6
9f	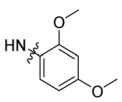	16.1 ± 1.1	19.7 ± 2.7
9g	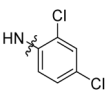	31.5 ± 4.2	64.5 ± 3.3
9h		32.5 ± 4.2	43.8 ± 2.5
9i	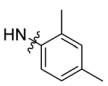	29.3 ± 6.6	51.5 ± 4.6
9j	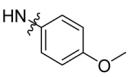	57.6 ± 5.7	68.1 ± 2.2
9k	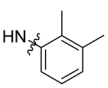	37.9 ± 0.14	53.5 ± 6.4
9l	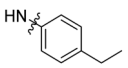	50.3 ± 6.7	65.3 ± 1.0
9m	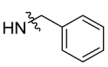	47.9 ± 2.7	72.3 ± 5.3
9n	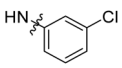	20.3 ± 2.0	34.3 ± 3.1
9o		48.9 ± 2.2	62.4 ± 3.7
Cisplatin	—	7.4 ± 1.6	15.2 ± 0.3
Doxorubicin	—	0.46 ± 0.02	0.59 ± 0.07

[a] Mean ± SD of 3–4 independent replicates. [b] A549; adenocarcinomic human alveolar basal epithelial cells. [c] SW480; primary colon cancer cells.

2.2. *In vitro* antiproliferative activity against cancer cells

The antiproliferative effects of the synthesized 2-(4-((2-(3,4,5-trimethoxyphenyl)-1*H*-benzo[*d*]imidazol-1-yl)methyl)-1*H*-1,2,3-triazol-1-yl)-*N*-substituted acetamides (**9a–o**) were tested on A549 (human lung cancer) and SW480 (human colon cancer) cell lines. The calculated IC_{50} values are presented in Table 1. Cisplatin and doxorubicin were used as the positive controls.

All the derivatives, except **9d**, demonstrated good antiproliferative activity against A549 and SW480 cells at the tested concentrations. Compound **9f**, bearing 2,4-dimethoxyphenyl substitution, was the most potent antiproliferative derivative with IC_{50} values of 16.1 ± 1.1 and 19.7 ± 2.7 μM against A549 and SW480, respectively. Moreover, **9c**, **9e**, and **9n** derivatives (having 4-nitrophenyl, 2-chlorophenyl, and 3-chlorophenyl moieties, respectively) showed remarkable activity with IC_{50} values of 20.3–23.5 μM against A549 and 22.5–34.3 μM against SW480.

According to the results, a detailed structure–activity relationship is presented. Modifying the phenyl substitution in **9b** to the benzyl substitution (as in **9m**) enhanced the antiproliferative activity against both cancer cells. Therefore, it can be stated that increasing the distance between the amine function and the phenyl ring improved the activity. Any substituent insertion on the phenyl ring, except the bromine atom, enhanced the antiproliferative effect. Based on the results for compounds **9f** and **9j**, it appears that the methoxy substitution enhances the activity. Compound **9f**, bearing methoxy functions at the *ortho* and *para* positions of the phenyl ring, was the most antiproliferative compound against the two cancer cell lines. The methoxy groups may establish hydrophobic and hydrogen bonding interactions with the potential receptors. Placing the electron-withdrawing nitro group at the *para* position caused **9c** to have high activity probably by providing hydrogen bonding interactions. It may be concluded that lipophilicity and steric hindrance are the determining factors for the antiproliferative activity of the *para*-substituted derivatives. Embedding the lipophilic and bulky bromine atom at the *para* position (as in **9d**) diminished the activity. In the case of methyl-substituted derivatives (**9a**, **9i**, and **9k**), the addition of two methyl groups on the phenyl ring would improve the activity. Moreover, the activity was increased by changing the 4-methyl substitution (**9a**) to the 4-ethyl (**9l**).

Table 2 Cytotoxicity of **9c**, **9e**, **9f**, and **9n** against MRC-5 normal cells

	IC_{50}[a] (μM)	SI[c]	
Compound	MRC-5[b]	A549	SW480
9c	90.6 ± 0.6	3.8	4.0
9e	105.0 ± 7.1	4.7	3.4
9f	120.7 ± 6.7	7.5	6.1
9n	124.2 ± 0.4	6.1	3.6
Cisplatin	18.3 ± 2.1	2.5	1.2
Doxorubicin	0.39 ± 0.06	0.8	0.7

[a] Values are expressed as mean ± SD of three independent replicates. [b] MRC-5: human fetal lung fibroblast cells. [c] SI: selectivity index = IC_{50} of a compound in a normal cell line/IC_{50} of the same compound in a cancerous cell line.

2.3. *In vitro* cytotoxic activity against normal cells

The cytotoxicity of four derivatives having the highest antiproliferative potential against the cancer cell lines, **9c**, **9e**, **9f**, and **9n**, was assessed against MRC-5 as a normal human cell line. The positive controls, cisplatin and doxorubicin, were used for comparison. The selectivity indexes (SI) for each compound are presented in Table 2. The tested derivatives exhibited significantly superior cytotoxic selectivity than cisplatin and doxorubicin toward cancerous cells (A549 and SW480) over the normal cell line (MRC-5). Compound **9f** was the most selective derivative toward A549 and SW480 cells with SI values of 7.5 and 6.1, respectively.

2.4. Cell cycle arrest

To investigate the effect of compound **9f** on the distribution of A549 cells across different phases of the cell cycle, the PI staining assay was performed. After 24 h treatment with 16.1 μM of **9f**, some changes in the number of cells in the cell cycle phases were observed; however, the variations were not significant compared to the control cells. Notably, after 48 h of treatment with 16.1 μM of **9f**, there was a significant increase in the number of cells in the S phase (33.04%, $p < 0.001$), along with a significant reduction in the number of cells in the G0/G1 phase (54.91%, $p < 0.01$), and a non-significant decrease in the G2/M phase (12.05%) as compared to the untreated control cells which showed 15.42%, 67.93%, and 16.65% of cells in S, G0/G1, and G2/M phases of the cell cycle, respectively (Fig. 2). This indicates that compound **9f** induces cell cycle arrest at the S phase in A549 cells.

2.5. Apoptosis induction

The apoptotic cell rates were determined for the A549 cells after treatment with derivative **9f** at a concentration of 16.1 μM for 24 and 48 h. The results are displayed in Fig. 3. To clarify the mechanism of **9f**-induced cell death in cells, flow cytometry detection of Annexin V-FITC/PI staining on the A549 cells was carried out. Compound **9f** significantly ($p < 0.001$) induced early and late apoptosis in A549 cells after 48 h as compared with the untreated control cells. The rates of early and late apoptosis increased over time, rising from 3.79% and 1.63% at 24 h to 12.2% and 4.01% at 48 h, respectively. The results revealed that **9f** increased the cellular apoptosis in a time-dependent manner.

2.6. *In silico* prediction of pharmacokinetic and toxicity properties

Pharmacokinetics profiles, including gastrointestinal (GI) absorption, *in vitro* Caco-2 cell permeability, *in vitro* plasma protein binding (PPB), P-glycoprotein (P-gp) inhibition, and *in vivo* blood–brain barrier (BBB) penetration, were predicted for the **9f** derivative. The results are presented in Table 3. Compound **9f** showed high GI absorption and had no BBB permeation; therefore, it can be stated that **9f** may be applied as

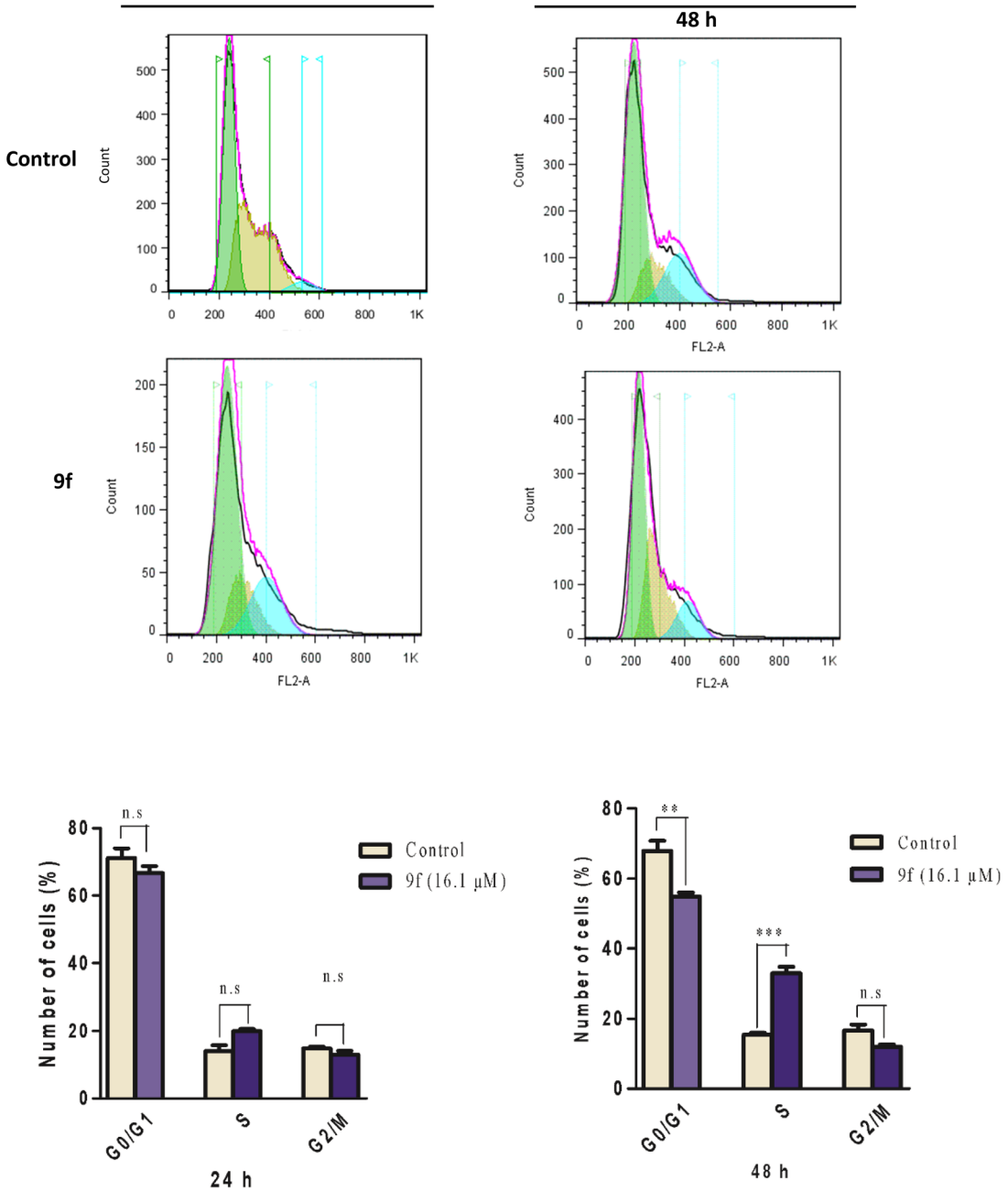

Fig. 2 Flow cytometry analysis of cell-cycle progression of A549 cells after treatment with compound **9f** for 24 h and 48 h. Data are the mean ± SD of three independent experiments. n.s: non-significant; $^{**}p < 0.01$; and $^{***}p < 0.001$; by one-way ANOVA and Tukey's *post hoc* test to compare the percentages of treated cells with the control cells.

an oral drug, and it is less likely to cause neurotoxicity. The compound was predicted to have strong PPB. Moreover, moderate human colorectal carcinoma cell permeability was assessed for **9f**. The compound was predicted to exhibit P-gp inhibition; therefore, it may have the potential to overcome multidrug resistance (MDR). P-gp is overexpressed in cancer cells and recognized as the key efflux transporter responsible for MDR to chemotherapeutics.[61–63] The predicted toxicities contain carcinogenicity with the mouse (Carcino-Mouse), human ether-a-go-go inhibition (hERG-inhibition), *in vitro* Ames test with (+S9) and without (−S9) metabolic activation in TA100 and TA1535 strains rat liver (TA100-10RLI, TA100-NA, TA1535-10RLI, and TA1535-NA). Compound **9f** showed negative carcinogenicity for the mouse and had a medium risk for hERG inhibition. The compound exhibited negative Ames mutagenicity to all the strains. Considering all the above-mentioned results, **9f** could be suggested as a promising candidate for further development as an anticancer agent.

2.7. Molecular docking

Type II topoisomerase (Topo II) is a predominant enzyme responsible for regulating DNA supercoiling and supercoiling

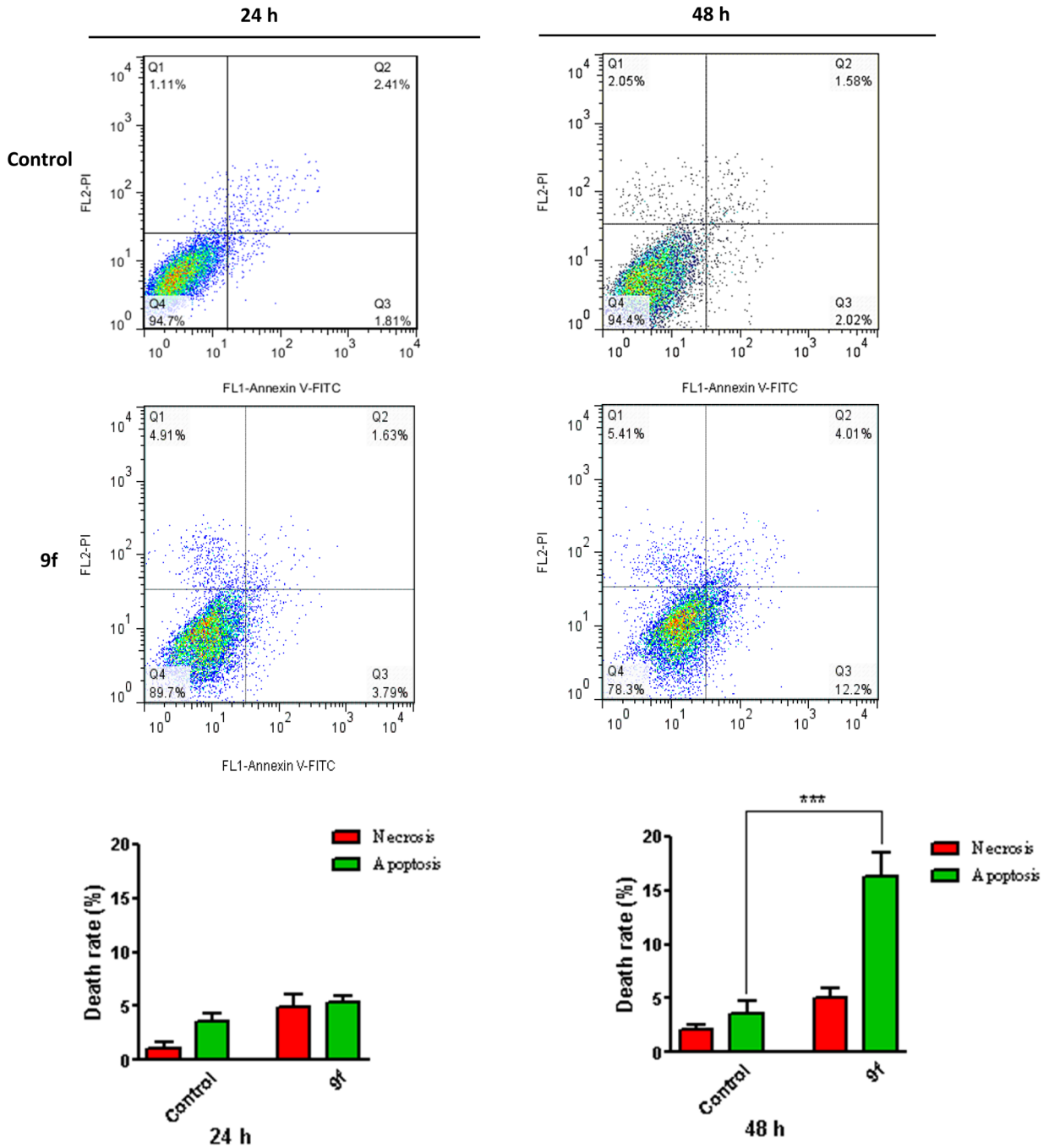

Fig. 3 Representation of the induced cell apoptosis by compound **9f**. Scatter plots were obtained by flow cytometry detection of Annexin V-FITC/PI staining on the A549 cells treated with 16.1 μM concentration of **9f** for 24 h and 48 h. Data are the mean ± SD of three independent experiments. ***$p < 0.001$; by one-way ANOVA and Tukey's *post hoc* test to compare the percentages of treated cells with the control cells.

Table 3 The drug-likeness and pharmacokinetic properties predicted results for **9f**

Pharmacokinetics						Toxicity					
Code	GI absorption	BBB	P-gp inhibition	Caco-2[a]	PPB[b]	Carcino-mouse	hERG-inhibition	TA100-10RLI	TA100-NA	TA1535-10RLI	TA1535-NA
9f	High	No	Yes	40.55	92.32	Negative	Medium-risk	Negative	Negative	Negative	Negative

[a] *In vitro* Caco-2 (human colorectal carcinoma) cell permeability (nm s^{-1}); low: <4, moderate: 4–70, high: >70. [b] *In vitro* plasma protein binding (percentage); strongly: >90, weakly: <90.

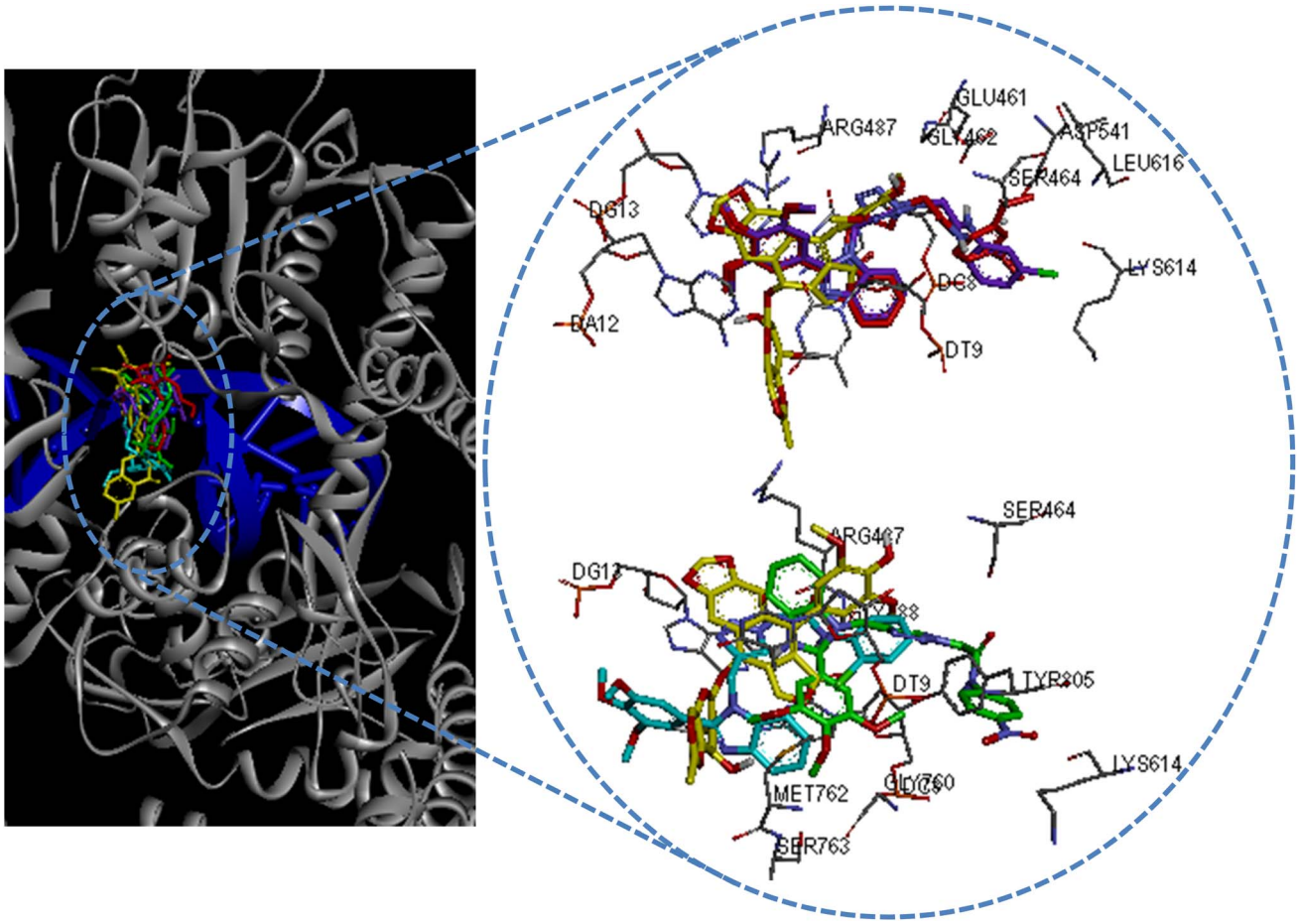

Fig. 4 Superimposition of binding modes of etoposide (yellow), **9c** (green), **9e** (cyan), **9f** (red), and **9n** (purple) within the binding site of Topo II-DNA (PDB ID: 5GWK).

and resolving DNA entanglements. It is involved in cellular processes, including DNA replication, recombination, and repair.[64] Due to its significant function in the cell life cycle, Topo II has become a prominent target for anticancer drug research.[65] Over the past few decades, several Topo II inhibitors, such as etoposide and doxorubicin, have been clinically applied as anticancer treatments. Topo II inhibitors are classified into two categories based on their mechanisms of action: Topo II poisons stabilize the covalent DNA-Topo II cleavable complexes, while catalytic inhibitors interfere with other steps in the catalytic cycle.[66]

Several derivatives of benzimidazole have been identified as efficient Topo II inhibitors. Biological and *in silico* studies have revealed that benzimidazole-containing derivatives may act as either poison or catalytic inhibitors of Topo II.[34,59,67–70] Bielawski *et al.* reported bis-benzimidazoles as Topo II inhibitors that interact with the GC base pair at the DNA minor groove.[69] Li *et al.* introduced two benzimidazole–rhodanine conjugates as non-intercalative Topo II inhibitors that bind to the ATP-binding site of the Topo II enzyme.[68] An antiproliferative benzimidazole–hydrazine conjugate was discovered to inhibit Topo II, arrest the cell cycle at the S phase, and induce

Table 4 Binding energies of the co-crystallized ligands and the most potent benzimidazole–triazoles with Topo II enzymes

	Binding energies (kcal mol^{-1})	
Compounds	Human Topo IIα-DNA (5GWK)	Human Topo IIα ATPase-no DNA (1ZXM)
ANP (innate ligand)	—	−10.7
Etoposide (innate ligand)	−11.1	—
9c	−10.3	−9.1
9e	−10.5	−8.7
9f	−11.0	−8.6
9n	−10.7	−9.4

apoptosis.[70] Most recently, a benzimidazole–triazole derivative has been reported as a potent Topo II inhibitor, showing an IC_{50} value of 2.52 μM, which arrested growth during the S phase and induced apoptosis in HepG-2 cancer cells.[59]

The molecular docking studies were carried out to predict the binding affinity of the most potent antiproliferative benzimidazole–triazole derivatives with the central domain of Topo II-DNA (PDB ID: 5GWK) and the ATPase domain of Topo II (PDB IDs: 1ZXM). The estimated binding energies of the co-crystallized ligands and the benzimidazole derivatives in the active sites of 5GWK and 1ZXM are presented in Table 4. RMSD values of 0.6 Å and 1.4 Å for 5GWK and 1ZXM, respectively, (<2.0 Å) proved that the top-ranked conformer of the ligands superimposed well over the corresponding X-ray crystallographic one

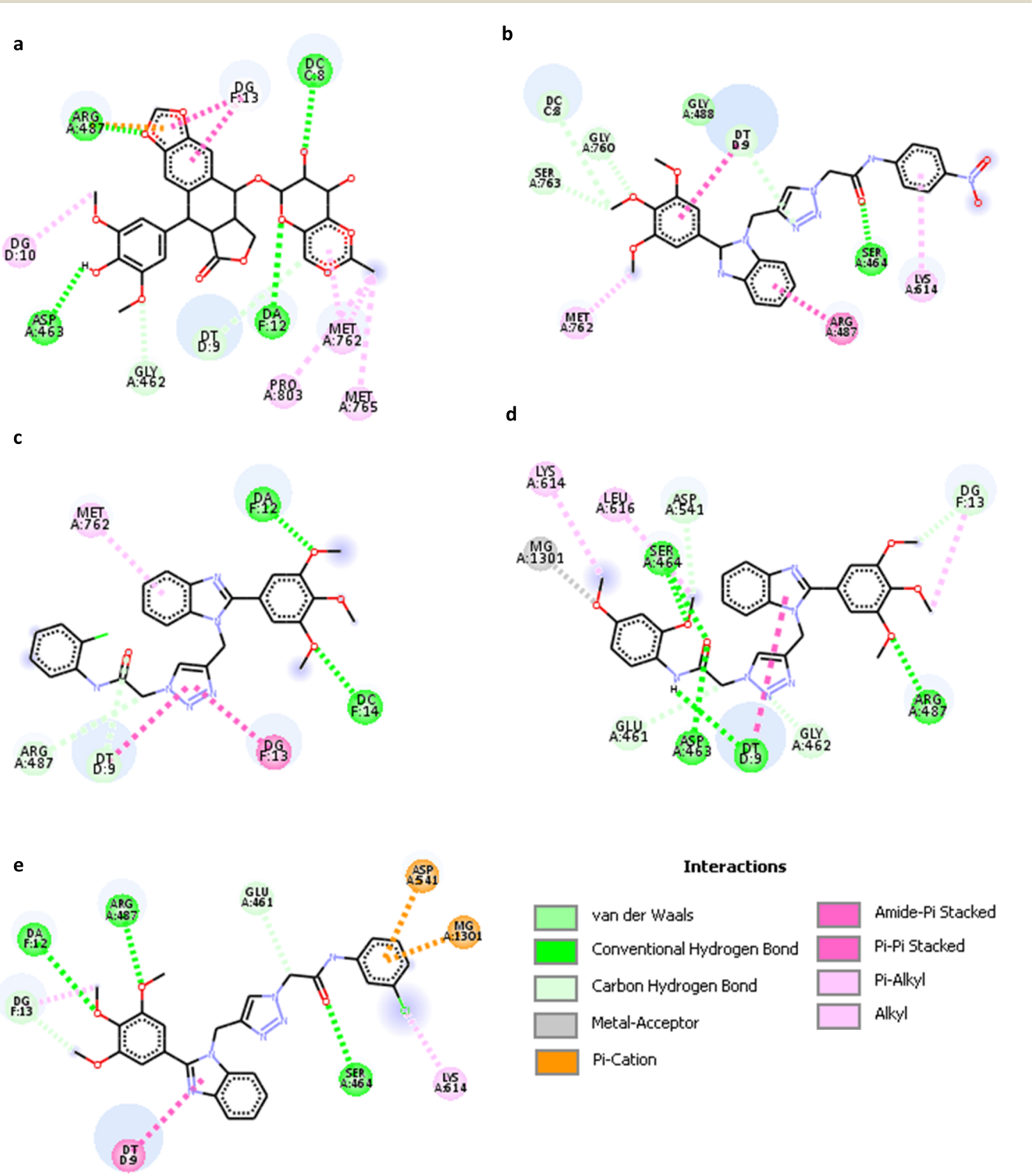

Fig. 5 Interactions of etoposide (a), **9c** (b), **9e** (c), **9f** (d), and **9n** (e) within the binding site of Topo II-DNA (PDB ID: 5GWK).

into the binding site of the enzymes. According to the predicted binding energies, benzimidazole–triazoles preferentially targeted Topo IIα-DNA (ΔGs = from −10.3 to −11.0 kcal mol^{-1}) rather than the ATPase domain of Topo IIα (ΔGs = from −8.6 to −9.4 kcal mol^{-1}) (Table 4).

The compounds accommodated well in the binding site of Topo II while occupying the DNA minor groove, as illustrated in Fig. 4. Compounds **9f** and **9n** possessed the same binding mode, while **9c** and **9e** oriented differently in the binding site. The interactions of **9c**, **9e**, **9f**, **9n**, and etoposide in complex with Topo IIα-DNA are illustrated in Fig. 5. Etoposide exhibited a binding energy of kcal mol^{-1} and illustrated various binding interactions in the active site. It formed hydrogen bonding interactions with ASP463, ARG487, DC8, and DA12. Moreover, etoposide established an electrostatic interaction with ARG487 and hydrophobic interactions with MET762, MET765, PRO803, DG13, and DG10 (Fig. 5a). Docking analysis of **9c** (Fig. 5b) represented a hydrogen bonding interaction with SER464 and hydrophobic interactions with ARG48, MET762, and LYS614. In the case of compound **9e**, hydrogen bonding interactions with DA12 and DC14, as well as hydrophobic interactions with MET762, DT9, and DG13 were observed (Fig. 5c). Compounds **9c** and **9e** are oriented in the binding pocket in such a way that the 4-nitrophenyl and 2-chlorophenyl substitutions did not participate in the formation of any interaction. In contrast, in compounds **9f** and **9n**, the 2,4-dimethoxyphenyl and 2-chlorophenyl moieties provided a variety of interactions. Compound **9f** possessed the most negative binding energy value (−11.0 kcal mol^{-1}) among other benzimidazole–triazoles, which was almost equal to that of etoposide. The compound was discovered to establish five hydrogen bonding interactions with ASP463, SER464, and ARG487 amino acids, as well as a stacking interaction with LYS614, LEU616, DT9, and DG13 nucleotides, besides a metal–acceptor interaction with MG1301 (Fig. 5d). Compound **9n** stabilized within the binding site by three hydrogen bonding interactions with SER464, ARG487, and DA12, hydrophobic interactions with LYS614, DT9, and DA12, and two electrostatic interactions with ASP451 and MG1301 (Fig. 5e).

3. Conclusions

New benzimidazole–triazole acetamides (**9a–o**) were designed and synthesized as anticancer agents. The derivatives were tested for their antiproliferative effect against cancerous (A549 and SW480) cells. Derivative **9f**, having a 2,4-dimethoxyphenyl, has the highest activity among all the tested compounds. Remarkably, it showed lower cytotoxicity compared to cisplatin and doxorubicin towards MRC-5 normal cells. This compound efficiently arrested A549 cells at the S phase and induced apoptosis at early and late stages after 48 h of treatment at the IC_{50} concentration. Finally, suitable pharmacokinetic profiling and low toxic effects were predicted *in silico* for the compound. This investigation identifies novel benzimidazole–triazole acetamide hybrids and highlights the potential of **9f** as a new anticancer agent. Further complementary studies on this subject would afford one step forward to find a new chemotherapeutic drug.

4. Materials and methods

4.1. Apparatus

All chemicals and reagents were of commercial grade. The progress of the reactions was followed using pre-coated aluminum sheet thin layer chromatography (TLC) plates (Merck, silica gel 60-F254). The IR spectra were collected with a Nicolet FT-IR Magna 550 spectrometer (KBr disks). The nuclear magnetic resonance (NMR) spectra were recorded with a Bruker DRX-500 NMR spectrometer (^{1}H: 301 MHz, ^{13}C: 76 MHz) using DMSO-d_6 as solvent. Chemical shifts (δ) are expressed in parts per million (ppm), and J values are given in hertz (Hz). Melting points were determined with a Barnstead IA9300 system (Electrothermal, UK) and are uncorrected. Elemental analyses were carried out by a PerkinElmer 2400 CHN Elemental Analyzer and were within ±0.4% of the theoretical values for C, H, and N.

4.2. Chemistry

4.2.1. Preparation of 2-(3,4,5-trimethoxyphenyl)-1*H*-benzo[*d*]imidazole (3). A mixture containing 3,4,5-trimethoxybenzaldehyde **1** (20 mmol, 3.92 g), 1,2-phenylenediamine **2** (22 mmol, 2.38 g), and 1.1 equivalents of sodium metabisulfite in DMF (25 mL) was refluxed for 12 h. After cooling, 50 mL of water was added, followed by extraction with 3 portions of 35 mL of ethyl acetate. The organic phase was dehydrated using magnesium sulfate. After filtration, the solvent was evaporated under vacuum to yield 2-(3,4,5-trimethoxyphenyl)-1*H*-benzo[*d*]imidazole **3**.[71] Yield: 92%.

4.2.2. Synthesis of 1-(prop-2-yn-1-yl)-2-(3,4,5-trimethoxyphenyl)-1*H*-benzo[*d*]imidazole (5). 2-(3,4,5-Trimethoxyphenyl)-1*H*-benzo[*d*]imidazole **3** (10 mmol, 2.84 g) and potassium carbonate (15 mmol, 2.07 g) were dissolved in a minimum amount of DMF and stirred at room temperature (rt) for 15 min. Propargyl bromide **4** (15 mmol, 1.78 g) was added to this solution and stirred for 24 h at rt. After completion of the reaction, the mixture was poured into ice-cold water. The solid product was filtered and dried to afford 1-(prop-2-yn-1-yl)-2-(3,4,5-trimethoxyphenyl)-1*H*-benzo[*d*]imidazole **5**. Yield: 90%; brown solid.[72]

4.2.3. Preparation of 2-chloro-*N*-substituted acetamide derivatives (8a–o). Aniline derivatives **6a–o** (50 mmol) were suspended in 25 mL of DMF and cooled to 0 °C. Then, chloroacetyl chloride **7** (65 mmol, 7.34 g) was added. The reaction mixture was stirred at rt for 24 h. Upon completion of the reaction, the reaction mixture was diluted with water, poured into crushed ice, and the obtained precipitate were filtered off. Finally, the residue was washed with water to obtain 2-chloro-*N*-substituted acetamide derivatives **8a–o**. Yield: 80–85%.[73]

4.2.4. Synthesis of *N*-substituted-2-(4-((2-(3,4,5-trimethoxyphenyl)-1*H*-benzo[*d*]imidazol-1-yl)methyl)-1*H*-1,2,3-triazol-1-yl) acetamides (9a–o). Corresponding acetamide **8a–o** (1.2 mmol), K_2CO_3 (1.5 mmol, 0.21 g), and NaN_3 (1.5 mmol, 0.97

g) were dissolved in DMF solvent and stirred at rt for 1 h. Then, copper sulfate pentahydrate ($CuSO_4 \cdot 5H_2O$) (0.15 mmol, 0.04 g), sodium ascorbate (0.45 mmol, 0.09 g), and the propargylated compound **5** (1 mmol, 0.32 g) were added to the reaction mixture. After the completion of the reaction, copper ions were removed from the mixture using a 0.05 M solution of ethylenediaminetetraacetic acid (EDTA). Then, the resulting precipitate was filtered and washed several times with water, and crystallized by EtOH to obtain the pure *N*-substituted-2-(4-((2-(3,4,5-trimethoxyphenyl)-1*H*-benzo[*d*]imidazol-1-yl)methyl)-1*H*-1,2,3-triazol-1-yl)acetamide derivatives **9a–o**.[34]

*4.2.4.1 N-(p-Tolyl)-2-(4-((2-(3,4,5-trimethoxyphenyl)-1H-benzo[d]imidazol-1-yl)methyl)-1H-1,2,3-triazol-1-yl)acetamide (**9a**).* Cream solid; yield: 80%; MP: 193–195 °C; IR (KBr, ν_{max}): 3310 (NH), 3035 (CH Aromatic), 2880 (CH Aliphatic), 1664 (C=O) cm^{-1}; ^{1}H NMR (301 MHz, DMSO-d_6) δ 10.40 (s, 1H), 8.27 (s, 1H), 7.73 (s, 2H), 7.47 (d, J = 8.1 Hz, 2H), 7.36–7.25 (m, 4H), 7.14 (d, J = 8.1 Hz, 2H), 5.64 (s, 2H), 5.33 (s, 2H), 3.86 (s, 6H), 3.79 (s, 3H), 2.27 (s, 3H) ppm; ^{13}C NMR (76 MHz, DMSO-d_6) δ 164.30, 153.50, 143.16, 139.22, 136.35, 133.24, 129.76, 125.89, 125.72, 123.08, 122.71, 119.68, 111.52, 107.43, 60.62, 56.59, 52.73, 20.91 ppm; anal. calcd for $C_{28}H_{28}N_6O_4$: C, 65.61; H, 5.51; N, 16.52. Found: C, 65.73; H, 5.69; N, 16.63.

*4.2.4.2 N-Phenyl-2-(4-((2-(3,4,5-trimethoxyphenyl)-1H-benzo[d]imidazol-1-yl)methyl)-1H-1,2,3-triazol-1-yl)acetamide (**9b**).* Cream solid; yield: 81%; MP: 189–1191 °C; IR (KBr, ν_{max}): 3315 (NH), 3020 (CH Aromatic), 2875 (CH Aliphatic), 1661 (C=O) cm^{-1}; ^{1}H NMR (301 MHz, DMSO-d_6) δ 10.49 (s, 1H), 8.28 (s, 1H), 7.73 (s, 2H), 7.59 (d, J = 7.4 Hz, 2H), 7.42–7.26 (m, 6H), 7.20–7.05 (m, 1H), 5.65 (s, 2H), 5.37 (s, 2H), 3.86 (s, 6H), 3.79 (s, 3H) ppm; ^{13}C NMR (76 MHz, DMSO-d_6) δ 164.58, 153.50, 143.18, 142.92, 139.24, 138.88, 129.40, 125.91, 125.65, 124.27, 123.12, 122.76, 119.69, 119.57, 111.56, 111.52, 107.47, 60.62, 56.59, 52.77 ppm; anal. calcd for $C_{27}H_{26}N_6O_4$: C, 65.05; H, 5.26; N, 16.86. Found: C, 65.21; H, 5.42; N, 17.02.

*4.2.4.3 N-(2-Nitrophenyl)-2-(4-((2-(3,4,5-trimethoxyphenyl)-1H-benzo[d]imidazol-1-yl)methyl)-1H-1,2,3-triazol-1-yl)acetamide (**9c**).* Khaki solid; yield: 77%; MP: 231–233 °C; IR (KBr, ν_{max}): 3375 (NH), 3065 (CH Aromatic), 2930 (CH Aliphatic), 1671 (C=O) cm^{-1}; ^{1}H NMR (301 MHz, DMSO-d_6) δ 11.17 (s, 1H), 8.31 (s, 1H), 8.26 (d, J = 8.3 Hz, 2H), 7.86 (s, 1H), 7.72 (s, 2H), 7.37–7.26 (m, 4H), 5.67 (s, 2H), 5.48 (s, 2H), 3.86 (s, 6H), 3.80 (s, 3H) ppm; ^{13}C NMR (76 MHz, DMSO-d_6) δ 165.77, 153.51, 144.99, 143.26, 143.05, 142.79, 139.26, 136.22, 125.93, 125.56, 123.18, 122.81, 119.49, 111.51, 107.44, 60.61, 56.56, 52.89 ppm; anal. calcd for $C_{27}H_{26}N_6O_4$: C, 59.66; H, 4.64; N, 18.04. Found: C, 59.82; H, 4.79; N, 18.23.

*4.2.4.4 N-(4-Bromophenyl)-2-(4-((2-(3,4,5-trimethoxyphenyl)-1H-benzo[d]imidazol-1-yl)methyl)-1H-1,2,3-triazol-1-yl)acetamide (**9d**).* Cream solid; yield: 74%; MP: 201–203 °C; IR (KBr, ν_{max}): 3335 (NH), 3030 (CH Aromatic), 2860 (CH Aliphatic), 1666 (C=O) cm^{-1}; ^{1}H NMR (301 MHz, DMSO-d_6) δ 10.66 (s, 1H), 8.30 (s, 1H), 7.73 (s, 2H), 7.60–7.53 (m, 4H), 7.38–7.27 (m, 4H), 5.67 (s, 2H), 5.39 (s, 2H), 3.89 (s, 6H), 3.81 (s, 3H) ppm; ^{13}C NMR (76 MHz, DMSO-d_6) δ 164.84, 153.51, 153.36, 143.25, 143.00, 139.21, 138.26, 136.30, 132.25, 125.90, 125.71, 123.08, 122.73, 121.62, 119.59, 115.91, 111.48, 111.41, 107.44, 60.64, 56.60, 52.77 ppm; anal. calcd for $C_{27}H_{25}BrN_6O_4$: C, 56.16; H, 4.36; N, 14.55. Found: C, 56.32; H, 4.52; N, 14.71.

*4.2.4.5 N-(2-Chlorophenyl)-2-(4-((2-(3,4,5-trimethoxyphenyl)-1H-benzo[d]imidazol-1-yl)methyl)-1H-1,2,3-triazol-1-yl)acetamide (**9e**).* Khaki solid; yield: 78%; MP: 208–210 °C; IR (KBr, ν_{max}): 3350 (NH), 3045 (CH Aromatic), 2870 (CH Aliphatic), 1666 (C=O) cm^{-1}; ^{1}H NMR (301 MHz, DMSO-d_6) δ 10.09 (s, 1H), 8.27 (s, 1H), 7.80–7.67 (m, 3H), 7.54 (d, J = 8.0 Hz, 1H), 7.39–7.21 (m, 3H), 5.65 (s, 2H), 5.46 (s, 2H), 3.85 (s, 6H), 3.78 (s, 3H) ppm; ^{13}C NMR (76 MHz, DMSO-d_6) δ 165.28, 153.49, 143.16, 139.23, 134.60, 130.09, 128.04, 127.20, 126.74, 126.33, 125.95, 123.16, 122.75, 119.53, 111.58, 107.37, 60.59, 56.54, 52.46 ppm; anal. calcd for $C_{27}H_{25}ClN_6O_4$: C, 60.85; H, 4.73; N, 15.77. Found: C, 60.98; H, 4.92; N, 15.96.

*4.2.4.6 N-(2,4-Dimethoxyphenyl)-2-(4-((2-(3,4,5-trimethoxyphenyl)-1H-benzo[d]imidazol-1-yl)methyl)-1H-1,2,3-triazol-1-yl)acetamide (**9f**).* Khaki solid; yield: 80%; MP: 196–198 °C; IR (KBr, ν_{max}): 3280 (NH), 3015 (CH Aromatic), 2850 (CH Aliphatic), 1662 (C=O) cm^{-1}; ^{1}H NMR (301 MHz, DMSO-d_6) δ 9.64 (s, 1H), 8.26 (s, 1H), 7.73 (s, 2H), 7.70 (s, 1H), 7.37–7.23 (m, 4H), 6.66 (d, J = 2.7 Hz, 1H), 6.50 (m, 1H), 5.64 (s, 2H), 5.40 (s, 2H), 3.86 (s, 6H), 3.84 (s, 3H), 3.79 (s, 3H), 3.76 (s, 3H) ppm; ^{13}C NMR (76 MHz, DMSO-d_6) δ 164.48, 157.51, 153.49, 151.78, 143.13, 139.20, 125.89, 125.64, 123.80, 123.11, 122.74, 120.02, 119.56, 111.51, 107.43, 104.56, 99.34, 60.61, 56.56, 56.20, 55.76, 52.62 ppm; anal. calcd for $C_{29}H_{30}N_6O_6$: C, 62.36; H, 5.41; N, 15.05. Found: C, 62.57; H, 5.58; N, 15.19.

*4.2.4.7 N-(2,4-Dichlorophenyl)-2-(4-((2-(3,4,5-trimethoxyphenyl)-1H-benzo[d]imidazol-1-yl)methyl)-1H-1,2,3-triazol-1-yl)acetamide (**9g**).* Khaki solid; yield: 80%; MP: 216–218 °C; IR (KBr, ν_{max}): 3310 (NH), 3040 (CH Aromatic), 2880 (CH Aliphatic), 1669 (C=O) cm^{-1}; ^{1}H NMR (301 MHz, DMSO-d_6) δ 10.18 (s, 1H), 8.27 (s, 1H), 7.77 (d, J = 8.8 Hz, 2H), 7.71 (s, 2H), 7.44 (d, J = 6.6 Hz, 1H), 7.37–7.26 (m, 4H), 5.65 (s, 2H), 5.47 (s, 2H), 3.83 (s, 6H), 3.78 (s, 3H) ppm; ^{13}C NMR (76 MHz, DMSO-d_6) δ 165.01, 153.03, 142.65, 138.79, 135.28, 133.37, 129.78, 129.08, 127.71, 127.09, 126.79, 125.50, 122.81, 122.37, 119.03, 111.24, 106.93, 60.13, 56.06, 52.03 ppm; anal. calcd for $C_{27}H_{24}Cl_2N_6O_4$: C, 57.15; H, 4.26; N, 14.81. Found: C, 57.34; H, 4.47; N, 14.95.

*4.2.4.8 N-(2-Nitrophenyl)-2-(4-((2-(3,4,5-trimethoxyphenyl)-1H-benzo[d]imidazol-1-yl)methyl)-1H-1,2,3-triazol-1-yl)acetamide (**9h**).* Khaki solid; yield: 75%; MP: 226–228 °C; IR (KBr, ν_{max}): 3375 (NH), 3065 (CH Aromatic), 2930 (CH Aliphatic), 1671 (C=O) cm^{-1}; ^{1}H NMR (301 MHz, DMSO-d_6) δ 10.76 (s, 1H), 8.24 (s, 1H), 8.00 (d, J = 8.0 Hz, 1H), 7.81–7.64 (m, 4H), 7.43 (t, J = 7.6 Hz, 2H), 7.32–7.26 (m, 3H), 5.65 (s, 2H), 5.44 (s, 2H), 3.84 (s, 6H), 3.78 (s, 3H) ppm; ^{13}C NMR (76 MHz, DMSO-d_6) δ 165.35, 153.54, 144.98, 143.73, 143.09, 142.88, 139.20, 134.66, 130.77, 126.39, 126.01, 125.56, 123.29, 111.89, 107.74, 60.58, 56.54, 52.49 ppm; anal. calcd for $C_{27}H_{25}N_7O_6$: C, 59.66; H, 4.64; N, 18.04. Found: C, 59.82; H, 4.82; N, 18.20.

*4.2.4.9 N-(2,4-Dimethylphenyl)-2-(4-((2-(3,4,5-trimethoxyphenyl)-1H-benzo[d]imidazol-1-yl)methyl)-1H-1,2,3-triazol-1-yl)acetamide (**9i**).* Light brown solid; yield: 77%; MP: 188–190 °C; IR (KBr, ν_{max}): 3265 (NH), 3020 (CH Aromatic), 2865 (CH Aliphatic), 1665 (C=O) cm^{-1}; ^{1}H NMR (301 MHz, DMSO-d_6) δ 9.75 (s, 1H), 8.27 (s, 1H), 7.78–7.65 (m, 2H), 7.34 (s, 2H),

7.32–7.26 (m, 3H), 7.05 (s, 1H), 6.99 (d, J = 8.2 Hz, 1H), 5.64 (s, 2H), 5.38 (s, 2H), 3.86 (s, 6H), 3.79 (s, 3H), 2.25 (s, 3H), 2.18 (s, 3H) ppm; ^{13}C NMR (76 MHz, DMSO-d_6) δ 164.70, 153.49, 143.15, 142.90, 139.22, 136.19, 135.20, 133.34, 132.04, 131.41, 127.04, 125.85, 125.62, 125.26, 123.10, 122.76, 119.54, 111.48, 107.46, 60.62, 56.57, 52.45, 20.92, 18.15 ppm; anal. calcd for $C_{29}H_{30}N_6O_4$: C, 66.15; H, 5.74; N, 15.96. Found: C, 66.29; H, 5.91; N, 16.14.

*4.2.4.10 N-(4-Methoxyphenyl)-2-(4-((2-(3,4,5-trimethoxyphenyl)-1H-benzo[d]imidazol-1-yl)methyl)-1H-1,2,3-triazol-1-yl)acetamide (**9j**).* Khaki solid; yield: 79%; MP: 174–176 °C; IR (KBr, ν_{max}): 3295 (NH), 3010 (CH Aromatic), 2870 (CH Aliphatic), 1661 (C=O) cm^{-1}; ^{1}H NMR (301 MHz, DMSO-d_6) δ 10.35 (s, 1H), 8.27 (s, 1H), 7.72 (s, 2H), 7.49 (d, J = 9.0 Hz, 2H), 7.37–7.26 (m, 4H), 6.92 (d, J = 9.0 Hz, 2H), 5.64 (s, 2H), 5.31 (s, 2H), 3.85 (s, 6H), 3.78 (s, 3H), 3.74 (s, 3H) ppm; ^{13}C NMR (76 MHz, DMSO-d_6) δ 164.02, 156.02, 153.50, 143.09, 139.25, 133.76, 131.96, 125.90, 125.54, 123.18, 122.80, 121.23, 114.49, 111.57, 107.47, 60.61, 56.57, 55.63, 52.67 ppm; anal. calcd for $C_{28}H_{28}N_6O_5$: C, 63.63; H, 5.34; N, 15.90. Found: C, 63.81; H, 5.51; N, 16.02.

*4.2.4.11 N-(2,3-Dimethylphenyl)-2-(4-((2-(3,4,5-trimethoxyphenyl)-1H-benzo[d]imidazol-1-yl)methyl)-1H-1,2,3-triazol-1-yl)acetamide (**9k**).* Light brown solid; yield: 77%; MP: 191–193 °C; IR (KBr, ν_{max}): 3275 (NH), 3020 (CH Aromatic), 2870 (CH Aliphatic), 1664 (C=O) cm^{-1}; ^{1}H NMR (301 MHz, DMSO-d_6) δ 9.86 (s, 1H), 8.26 (s, 1H), 7.72 (s, 2H), 7.34–7.26 (m, 3H), 7.16 (d, J = 6.8 Hz, 1H), 7.10–7.00 (m, 3H), 5.64 (s, 2H), 5.38 (s, 2H), 3.85 (s, 6H), 3.78 (s, 3H), 2.26 (s, 3H), 2.09 (s, 3H) ppm; ^{13}C NMR (76 MHz, DMSO-d_6) δ 164.80, 153.49, 143.13, 139.19, 137.63, 135.69, 131.60, 131.52, 127.76, 125.88, 125.78, 123.72, 123.12, 122.74, 119.59, 111.56, 107.39, 60.61, 56.56, 52.41, 20.60, 14.44 ppm; anal. calcd for $C_{29}H_{30}N_6O_4$: C, 66.15; H, 5.74; N, 15.96. Found: C, 66.32; H, 5.81; N, 16.12.

*4.2.4.12 N-(4-Ethylphenyl)-2-(4-((2-(3,4,5-trimethoxyphenyl)-1H-benzo[d]imidazol-1-yl)methyl)-1H-1,2,3-triazol-1-yl)acetamide (**9l**).* Khaki solid; yield: 76%; MP: 196–198 °C; IR (KBr, ν_{max}): 3275 (NH), 3020 (CH Aromatic), 2870 (CH Aliphatic), 1664 (C=O) cm^{-1}; ^{1}H NMR (301 MHz, DMSO-d_6) δ 10.42 (s, 1H), 8.28 (s, 1H), 7.73 (s, 2H), 7.49 (d, J = 8.2 Hz, 2H), 7.37–7.23 (m, 4H), 7.17 (d, J = 8.1 Hz, 2H), 5.64 (s, 2H), 5.34 (s, 2H), 3.85 (s, 6H), 3.78 (s, 3H), 2.61–2.54 (m, 2H), 1.16 (t, J = 7.6 Hz, 3H) ppm; ^{13}C NMR (76 MHz, DMSO-d_6) δ 164.31, 153.50, 143.12, 139.67, 139.22, 136.55, 128.57, 125.91, 125.60, 123.13, 122.76, 119.75, 119.52, 111.53, 107.44, 60.61, 56.57, 52.71, 28.06, 16.10 ppm; anal. calcd for $C_{29}H_{30}N_6O_4$: C, 66.15; H, 5.74; N, 15.96. Found: C, 66.29; H, 5.93; N, 16.11.

*4.2.4.13 N-Benzyl-2-(4-((2-(3,4,5-trimethoxyphenyl)-1H-benzo[d]imidazol-1-yl)methyl)-1H-1,2,3-triazol-1-yl)acetamide (**9m**).* Khaki solid; yield: 74%; MP: 196–198 °C; IR (KBr, ν_{max}): 3290 (NH), 3030 (CH Aromatic), 2880 (CH Aliphatic), 1666 (C=O) cm^{-1}; ^{1}H NMR (301 MHz, DMSO-d_6) δ 8.86 (t, J = 5.8 Hz, 1H), 8.23 (s, 1H), 7.74 (s, 2H), 7.38–7.32 (m, 4H), 7.31–7.27 (m, 5H), 5.63 (s, 2H), 5.20 (s, 2H), 4.34 (d, J = 5.7 Hz, 2H), 3.85 (s, 6H), 3.79 (s, 3H) ppm; ^{13}C NMR (76 MHz, DMSO-d_6) δ 165.81, 153.51, 143.09, 139.21, 139.16, 128.84, 127.85, 127.49, 125.82, 123.11, 122.69, 119.67, 111.63, 107.38, 60.61, 56.57, 52.15, 42.84 ppm; anal. calcd for $C_{28}H_{28}N_6O_4$: C, 65.61; H, 5.51; N, 16.40. Found: C, 65.82; H, 5.79; N, 16.54.

*4.2.4.14 N-(3-Chlorophenyl)-2-(4-((2-(3,4,5-trimethoxyphenyl)-1H-benzo[d]imidazol-1-yl)methyl)-1H-1,2,3-triazol-1-yl)acetamide (**9n**).* Cream solid; yield: 76%; MP: 208–210 °C; IR (KBr, ν_{max}): 3345 (NH), 3060 (CH Aromatic), 2855 (CH Aliphatic), 1669 (C=O) cm^{-1}; ^{1}H NMR (301 MHz, DMSO-d_6) δ 10.10 (s, 1H), 8.28 (s, 1H), 7.79–7.67 (m, 3H), 7.54 (d, J = 7.9 Hz, 1H), 7.38–7.32 (m, 3H), 7.31–7.27 (m, 2H), 7.23 (t, J = 7.9 Hz, 1H), 5.65 (s, 2H), 5.48 (s, 2H), 3.86 (s, 6H), 3.79 (s, 3H) ppm; ^{13}C NMR (76 MHz, DMSO-d_6) δ 165.29, 153.50, 143.23, 139.21, 134.61, 130.10, 128.04, 127.20, 126.75, 126.34, 125.94, 123.11, 122.74, 119.58, 111.53, 107.41, 60.62, 56.57, 52.51 ppm; anal. calcd for $C_{27}H_{25}ClN_6O_4$: C, 60.85; H, 4.73; N, 15.77. Found: C, 61.03; H, 4.69; N, 15.95.

*4.2.4.15 N-(2-Fluorophenyl)-2-(4-((2-(3,4,5-trimethoxyphenyl)-1H-benzo[d]imidazol-1-yl)methyl)-1H-1,2,3-triazol-1-yl)acetamide (**9o**).* Cream solid; yield: 75%; MP: 211–213 °C; IR (KBr, ν_{max}): 3370 (NH), 3060 (CH Aromatic), 2850 (CH Aliphatic), 1668 (C=O) cm^{-1}; ^{1}H NMR (301 MHz, DMSO-d_6) δ 10.35 (s, 1H), 8.28 (s, 1H), 7.97–7.85 (m, 1H), 7.73 (s, 2H), 7.37–7.25 (m, 5H), 7.23–7.15 (m, 2H), 5.65 (s, 2H), 5.46 (s, 2H), 3.85 (s, 6H), 3.79 (s, 3H) ppm; ^{13}C NMR (76 MHz, DMSO-d_6) δ 165.22, 155.54, 153.50, 152.29, 143.16, 126.20, 126.10, 126.00, 125.96, 125.85, 124.20, 123.16, 122.75, 119.64, 116.21, 115.95, 111.59, 56.55, 52.54 ppm; anal. calcd for $C_{27}H_{25}FN_6O_4$: C, 62.78; H, 4.88; N, 16.27. Found: C, 62.95; H, 5.01; N, 16.41.

4.3. MTT assay

The cytotoxic activity of the designed compounds (**9a–o**) was assessed by the MTT (3-(4,5-dimethylthiazol-yl)-2,5-diphenyltetrazolium bromide) assay according to our previous procedure.[40,74,75] The standard drugs cisplatin and doxorubicin were used as the positive controls. Two human cancer cell lines, SW480 (human colon adenocarcinoma) and A549 (human lung adenocarcinoma), and the normal MRC-5 (human fetal lung fibroblast cells) cells were obtained from the National Cell Bank of Iran (NCBI, Pasteur Institute, Tehran, Iran). RPMI 1640 culture media was used to culture cancer cell lines. The media was supplemented with 10% fetal bovine serum (FBS) and 1% penicillin–streptomycin (Gibco, USA), and the cells were kept at 37 °C in a humidified CO_2 incubator. Trypsin/EDTA 0.5% solution (Gibco/USA) was applied to harvest cells, and the cells were seeded in 96-well microplates at a density of 8×10^3 cells per well. The cells were treated with different concentrations of the designed compounds, cisplatin, and doxorubicin in triplicate times. Three untreated wells were used as the negative control. After 72 h, the media was removed, and 100 μL fresh MTT solution was added to the wells. Then, the plates were incubated for 4 h at 37 °C to obtain formazan purple crystals. Finally, the media was removed, 150 μL DMSO was added, and incubated at 37 °C in the dark for 10 min to dissolve the crystals. The absorbance of individual wells was read at 490 nm using a microplate ELISA reader. Excel 2016 and Curve Expert 1.4 were used to analyze the data. The data are presented as mean ± SD of 3–4 independent experiments.

4.4. Cell cycle

The total number of 5×10^4 A549 cells were pre-cultured in 24 well plates in high glucose DMEM culture medium for 16 h in standard culturing conditions. After treatment of cells with 16.1 μM of **9f** for 24 h and 48 h, cells were harvested with 0.25% trypsin, followed by washing with PBS and stained with propidium iodide (5 μL, 1 mg mL^{-1}), and 1 U of RNase A. Cell cycle analysis was performed using flow cytometry (BD FACSCalibur Flow Cytometer, BD, USA). The DNA content was analyzed using FlowJo 10.0 software.

4.5. Apoptosis assay

1×10^5 of A549 cells were pre-cultured for 16 h followed by exposure to 16.1 μM of **9f** for 24 h and 48 h. Then, Annexin V/PI staining was performed using eBioscience™ Annexin V apoptosis detection kit (Invitrogen). Cells were washed once with phosphate-buffered saline (PBS), and once with 1000 μL 1× binding buffer. In the next step, the cells were suspended with 100 μL of binding buffer containing 5 μL of Annexin V-FITC for 15 min. Afterward, cells were washed again with 1000 μL binding buffer and resuspended in 200 μL of the same buffer containing 5 μL PI solution. The apoptosis rates were then determined by BD FACS Calibur™ flow cytometry (BD Biosciences, San Jose, CA, USA).

4.6. *In silico* pharmacokinetics and toxicities assessment

The pharmacokinetic and toxicity properties for compound **9f** was predicted *in silico* by preADMET online server (**http://preadmet.bmdrc.org/**) and SwissADME (**http://www.swissadme.ch**) free web tool.

4.7. Molecular docking

The structures of all the compounds were sketched, optimized, and energy minimized using the HyperChem software. The structures were converted to their "PDBQT" format using the Open Babel program. The three-dimensional structures of different human Topo II proteins (PDB IDs: 1ZXM and 5GWK) were obtained from the protein data bank (**http://www.rcsb.org**). To prepare the proteins for docking, heteroatoms were removed, polar hydrogens were added, and charges were assigned. The active sites were defined using grid boxes of appropriate sizes around the binding site of the co-crystallized ligands. The docking study was performed using the Autodock vina,[76] and the interactions were visualized using Discovery Studio 2021 Client.

Author contributions

A. S. S. A.: methodology, investigation. S. R.: conceptualization, methodology, supervision, editing and writing. M. H. S.: investigation, data curation. Z. D.: investigation, writing. A. M. T.: resources, validation. M. N.: formal analysis. N. D.: conceptualization. M. E.: formal analysis. S. S.: data curation. M. R. M.-T.: visualization. A. G.: formal analysis. B. L.: resources, validation. M. M.: methodology, conceptualization, supervision, project administration, editing. Y. G.: conceptualization, supervision, project administration.

Conflicts of interest

The authors declare no conflict of interest.

Data availability

The data supporting this article have been included in the supplementary information (SI). Supplementary information is available. See DOI: **https://doi.org/10.1039/d5ra02760h**.

Acknowledgements

This work was supported by the Vice-Chancellor for Research, Shiraz University of Medical Sciences, Iran (grant number: 31956).

References

1 F. Bray, M. Laversanne, H. Sung, J. Ferlay, R. L. Siegel, I. Soerjomataram and A. Jemal, *Ca-Cancer J. Clin.*, 2024, **74**, 229–263.
2 D. T. Debela, S. G. Muzazu, K. D. Heraro, M. T. Ndalama, B. W. Mesele, D. C. Haile, S. K. Kitui and T. Manyazewal, *SAGE Open Med.*, 2021, **9**, 20503121211034366.
3 J. B. Wright, *Chem. Rev.*, 1951, **48**, 397–541.
4 M. J. Akhtar, M. S. Yar, V. K. Sharma, A. A. Khan, Z. Ali, M. R. Haider and A. Pathak, *Curr. Med. Chem.*, 2020, **27**, 5970–6014.
5 Y. Bansal, R. Minhas, A. Singhal, R. K. Arora and G. Bansal, *Curr. Org. Chem.*, 2021, **25**, 669–694.
6 R. S. Keri, A. Hiremathad, S. Budagumpi and B. M. Nagaraja, *Chem. Biol. Drug Des.*, 2015, **86**, 19–65.
7 H. D. Attram, S. Wittlin and K. Chibale, *MedChemComm*, 2019, **10**, 450–455.
8 J. A. Romero, M. E. Acosta, N. D. Gamboa, M. R. Mijares, J. B. De Sanctis, L. J. Llovera and J. E. Charris, *Med. Chem. Res.*, 2019, **28**, 13–27.
9 M. F. AlAjmi, A. Hussain, A. Alsalme and R. A. Khan, *RSC Adv.*, 2016, **6**, 19475–19481.
10 X. J. Wang, M. Y. Xi, J. H. Fu, F. R. Zhang, G. F. Cheng and Q. D. You, *Chin. Chem. Lett.*, 2012, **23**, 707–710.
11 N. Siddiqui, M. S. Alam, R. Ali, M. S. Yar and O. Alam, *Med. Chem. Res.*, 2016, **25**, 1390–1402.
12 N. Singh, A. Pandurangan, K. Rana, P. Anand, A. Ahamad and A. K. Tiwari, *Int. Curr. Pharm. J.*, 2012, **1**, 119–127.
13 N. T. Chandrika, S. K. Shrestha, H. X. Ngo and S. Garneau-Tsodikova, *Bioorg. Med. Chem.*, 2016, **24**, 3680–3686.
14 S. H. Nile, B. Kumar and S. W. Park, *Chem. Biol. Drug Des.*, 2013, **82**, 290–295.
15 Q. McKellar and E. Scott, *J. Vet. Pharmacol. Ther.*, 1990, **13**, 223–247.
16 W. A. Denny, G. W. Rewcastle and B. C. Baguley, *J. Med. Chem.*, 1990, **33**, 814–819.

17 J. Valdez, R. Cedillo, A. Hernandez-Campos, L. Yepez, F. Hernandez-Luis, G. Navarrete-Vazquez, A. Tapia, R. Cortes, M. Hernández and R. Castillo, *Bioorg. Med. Chem. Lett.*, 2002, **12**, 2221–2224.
18 J. Chen, N. Li, B. Liu, J. Ling, W. Yang, X. Pang and T. Li, *Life Sci.*, 2020, **248**, 117469.
19 M. Ayoubi-Chianeh and M. Z. Kassaee, *Struct. Chem.*, 2020, **31**, 2041–2050.
20 P. Douglas, R. Ye, S. Radhamani, A. Cobban, N. P. Jenkins, E. Bartlett, J. Roveredo, A. N. Kettenbach and S. P. Lees-Miller, *Mol. Cell. Biol.*, 2020, **40**, e00191.
21 A. Das, J. L. Martinez Santos, M. Alshareef, G. B. F. Porto, L. K. Infinger, W. A. Vandergrift III, S. M. Lindhorst, A. K. Varma, S. J. Patel and D. Cachia, *Cancer Invest.*, 2020, **38**, 349–355.
22 S. Kopetz, A. Grothey, R. Yaeger, E. Van Cutsem, J. Desai, T. Yoshino, H. Wasan, F. Ciardiello, F. Loupakis and Y. S. Hong, *N. Engl. J. Med.*, 2019, **381**, 1632–1643.
23 A. M. Gross, P. L. Wolters, E. Dombi, A. Baldwin, P. Whitcomb, M. J. Fisher, B. Weiss, A. Kim, M. Bornhorst and A. C. Shah, *N. Engl. J. Med.*, 2020, **382**, 1430–1442.
24 G. W. Sledge, M. Toi, P. Neven, J. Sohn, K. Inoue, X. Pivot, O. Burdaeva, M. Okera, N. Masuda and P. A. Kaufman, *JAMA Oncol.*, 2020, **6**, 116–124.
25 S. Boussios, P. Karihtala, M. Moschetta, C. Abson, A. Karathanasi, N. Zakynthinakis-Kyriakou, J. E. Ryan, M. Sheriff, E. Rassy and N. Pavlidis, *Invest. New Drugs*, 2020, **38**, 181–193.
26 D. A. Bastos and E. S. Antonarakis, *Drug Des., Dev. Ther.*, 2016, 2289–2297.
27 D.-W. Kim, D. S.-W. Tan, S. Ponce Aix, L. V. Sequist, E. F. Smit, T. Hida, J. C.-H. Yang, E. Felip, T. Seto and C. Grohé, *J. Clin. Oncol.*, 2018, **36**, 9094.
28 P. Sharma, T. S. Reddy, D. Thummuri, K. R. Senwar, N. P. Kumar, V. Naidu, S. K. Bhargava and N. Shankaraiah, *Eur. J. Med. Chem.*, 2016, **124**, 608–621.
29 S. Nazreen, A. S. Almalki, S. E. I. Elbehairi, A. A. Shati, M. Y. Alfaifi, A. A. Elhenawy, N. I. Alsenani, A. Alfarsi, A. Alhadhrami and E. A. Alqurashi, *Molecules*, 2022, **27**, 6899.
30 Y. Li, C. Tan, C. Gao, C. Zhang, X. Luan, X. Chen, H. Liu, Y. Chen and Y. Jiang, *Bioorg. Med. Chem.*, 2011, **19**, 4529–4535.
31 A. Kamal, A. B. Shaik, S. Polepalli, G. B. Kumar, V. S. Reddy, R. Mahesh, S. Garimella and N. Jain, *Bioorg. Med. Chem.*, 2015, **23**, 1082–1095.
32 E. Oksuzoglu, B. Tekiner-Gulbas, S. Alper, O. Temiz-Arpaci, T. Ertan, I. Yildiz, N. Diril, E. Sener-Aki and I. Yalcin, *J. Enzyme Inhib. Med. Chem.*, 2008, **23**, 37–42.
33 T.-K.-C. Huynh, T.-H.-A. Nguyen, N.-H.-S. Tran, T.-D. Nguyen and T.-K.-D. Hoang, *J. Chem. Sci.*, 2020, **132**, 1–9.
34 N. Dastyafteh, M. Negahdaripour, M. H. Sayahi, M. Emami, Y. Ghasemi, E. Safaei, H. Azizian, Z. P. Jahromi, M. Asadi and M. R. Mohajeri-Tehrani, *RSC Adv.*, 2024, **14**, 35323–35335.
35 D. Dixit, P. K. Verma and R. K. Marwaha, *J. Iran. Chem. Soc.*, 2021, **18**, 2535–2565.
36 M. J. Vaishnani, S. Bijani, M. Rahamathulla, L. Baldaniya, V. Jain, K. Y. Thajudeen, M. M. Ahmed, S. A. Farhana and I. Pasha, *Green Chem. Lett. Rev.*, 2024, **17**, 2307989.
37 K. Kushwaha, N. Kaushik and S. C. Jain, *Bioorg. Med. Chem. Lett.*, 2014, **24**, 1795–1801.
38 L. Peyton, S. Gallagher and M. Hashemzadeh, *Drugs Today*, 2015, **51**, 705–718.
39 K. I. Slavova, L. T. Todorov, N. P. Belskaya, M. A. Palafox and I. P. Kostova, *Recent Pat. Anti-Cancer Drug Discovery*, 2020, **15**, 92–112.
40 M. Gholampour, S. Ranjbar, N. Edraki, M. Mohabbati, O. Firuzi and M. Khoshneviszadeh, *Bioorg. Chem.*, 2019, **88**, 102967.
41 D. Verbanac, R. Malik, M. Chand, K. Kushwaha, M. Vashist, M. Matijašić, V. Stepanić, M. Perić, H. Č. Paljetak and L. Saso, *J. Enzyme Inhib. Med. Chem.*, 2016, **31**, 104–110.
42 R. Kharb, M. Shahar Yar and P. Chander Sharma, *Mini-Rev. Med. Chem.*, 2011, **11**, 84–96.
43 G. E.-D. A. A. Abuo-Rahma, M. Abdel-Aziz, E. A. Beshr and T. F. Ali, *Eur. J. Med. Chem.*, 2014, **71**, 185–198.
44 T. George, D. Mehta, R. Tahilramani, J. David and P. Talwalker, *J. Med. Chem.*, 1971, **14**, 335–338.
45 J. Liu, Q. Liu, X. Yang, S. Xu, H. Zhang, R. Bai, H. Yao, J. Jiang, M. Shen and X. Wu, *Bioorg. Med. Chem.*, 2013, **21**, 7742–7751.
46 S. Ranjbar, P. s. Shahvaran, N. Edraki, M. Khoshneviszadeh, M. Darroudi, Y. Sarrafi, M. Hamzehloueian and M. Khoshneviszadeh, *Arch. Pharm.*, 2020, **353**, 2000058.
47 M. Darroudi, S. Ranjbar, M. Esfandiar, M. Khoshneviszadeh, M. Hamzehloueian, M. Khoshneviszadeh and Y. Sarrafi, *Appl. Organomet. Chem.*, 2020, **34**, e5962.
48 M. Mahdavi, A. Ashtari, M. Khoshneviszadeh, S. Ranjbar, A. Dehghani, T. Akbarzadeh, B. Larijani, M. Khoshneviszadeh and M. Saeedi, *Chem. Biodiversity*, 2018, **15**, e1800120.
49 Z. Fallah, M. Tajbakhsh, M. Alikhani, B. Larijani, M. A. Faramarzi, H. Hamedifar, M. Mohammadi-Khanaposhtani and M. Mahdavi, *J. Mol. Struct.*, 2022, **1255**, 132469.
50 K. N. Ankali, J. Rangaswamy, M. Shalavadi, N. Naik and G. naik Krishnamurthy, *J. Mol. Struct.*, 2021, **1236**, 130357.
51 G. S. Kumar, Y. Rajendraprasad, B. Mallikarjuna, S. Chandrashekar and C. Kistayya, *Eur. J. Med. Chem.*, 2010, **45**, 2063–2074.
52 K. Pedrood, F. Taayoshi, A. Moazzam, A. Iraji, A. Yavari, S. Ansari, S. M. Sajjadi-Jazi, M. R. Mohajeri-Tehrani, N. Garmsiri and V. Haghpanah, *Heliyon*, 2023, **9**, e13528.
53 M. Vaishnani, A. Prajapati, S. Bijani, S. Shah, M. Kamal, M. Alsaweed, V. Jain and D. Iqbal, *Polycyclic Aromat. Compd.*, 2025, 1–25.
54 M. Vaishnani, *Antibiotics*, 2023, **12**, 1220.
55 M. A. Soliman, E. H. Eltamany, A. T. Boraei, M. R. Aouad, A. Aljuhani, B. Almohaywi, A. A. Awaji, R. Alghamdi, A. K. Aljohani and H. E. Ahmed, *ChemistrySelect*, 2025, **10**, e202500813.
56 M. Eser and İ. Çavuş, *Vet. Sci.*, 2023, **10**, 648.

57 F. Yılmaz, E. Mentese and N. Baltas, *Lett. Drug Des. Discovery*, 2017, **14**, 201–208.
58 U. Acar Cevik, B. N. Saglik, S. Levent, D. Osmaniye, B. Kaya Cavuşoglu, Y. Ozkay and Z. A. Kaplancikli, *Molecules*, 2019, **24**, 861.
59 D. I. Othman, A. Hamdi, S. S. Tawfik, A. A. Elgazar and A. S. Mostafa, *J. Enzyme Inhib. Med. Chem.*, 2023, **38**, 2166037.
60 V. V. Rostovtsev, L. G. Green, V. V. Fokin and K. B. Sharpless, A Stepwise Huisgen Cycloaddition Process: Copper(I)-Catalyzed Regioselective "Ligation" of Azides and Terminal Alkynes, *Angew. Chem., Int. Ed.*, 2002, **41**, 2596–2599.
61 S. Ranjbar, R. Khonkarn, A. Moreno, H. Baubichon-Cortay, R. Miri, M. Khoshneviszadeh, L. Saso, N. Edraki, P. Falson and O. Firuzi, *Toxicol. Appl. Pharmacol.*, 2019, **362**, 136–149.
62 S. Ranjbar, F. F. Lashkarian, M. Khoshneviszadeh, F. Moosavi, A. Sakhteman, F. Zargari, L. Saso, O. Firuzi and N. Edraki, *J. Mol. Struct.*, 2023, **1285**, 135427.
63 S. Ranjbar, O. Firuzi, N. Edraki, O. Shahraki, L. Saso, M. Khoshneviszadeh and R. Miri, *MedChemComm*, 2017, **8**, 1919–1933.
64 J. L. Nitiss, *Nat. Rev. Cancer*, 2009, **9**, 327–337.
65 Y. Pommier, Y. Sun, S.-y. N. Huang and J. L. Nitiss, *Nat. Rev. Mol. Cell Biol.*, 2016, **17**, 703–721.
66 A. O. Akinyemi, J. da Silveira Rocha, G. P. de Oliveira, J. de Jesus Santos, B. C. D. Owoyemi and F. V. Rocha, *Mini-Rev. Med. Chem.*, 2025, **25**, 891–910.
67 W. Zhou, W. Zhang, Y. Peng, Z.-H. Jiang, L. Zhang and Z. Du, *Molecules*, 2020, **25**, 3180.
68 P. Li, W. Zhang, H. Jiang, Y. Li, C. Dong, H. Chen, K. Zhang and Z. Du, *MedChemComm*, 2018, **9**, 1194–1205.
69 K. Bielawski, S. Wolczynski and A. Bielawska, *Pol. J. Pharmacol.*, 2004, **56**, 373–378.
70 N. A. Nawareg, A. S. Mostafa, S. M. El-Messery and M. N. Nasr, *Bioorg. Chem.*, 2022, **127**, 106038.
71 M. K. Ghomi, N. Dastyafteh, M. N. Montazer, M. Noori, S. Mojtabavi, M. A. Faramarzi, S. M. Hashemi and M. Mahdavi, *Sci. Rep.*, 2024, **14**, 501.
72 Q. Yang, T. Xu and Z. Yu, *Org. Lett.*, 2014, **16**, 6310–6313.
73 M. Noori, A. Davoodi, A. Iraji, N. Dastyafteh, M. Khalili, M. Asadi, M. Mohammadi Khanaposhtani, S. Mojtabavi, M. Dianatpour and M. A. Faramarzi, *Sci. Rep.*, 2022, **12**, 14019.
74 S. Ranjbar, M. Khoshneviszadeh, M. Tavakkoli, R. Miri, N. Edraki and O. Firuzi, *Mol. Diversity*, 2021, 1–20.
75 S. Ranjbar, P. Sadeghian, S. Khademian, M. Emami, Z. P. Jahromi, S. H. Mirmajidi, F. Zare, M. Negahdaripour, Y. Ghasemi and M. Khoshneviszadeh, *Heliyon*, 2024, **10**, e29850.
76 O. Trott and A. J. Olson, *J. Comput. Chem.*, 2010, **31**, 455–461.